Estimation and Use of Prior Information in FEM-CSI for Biomedical Microwave Tomography

Amer Zakaria, *Member, IEEE*, Anastasia Baran, and Joe LoVetri, *Senior Member, IEEE*

(Invited Paper)

***Abstract*—Prior information is used to improve imaging results obtained using the finite-element contrast source inversion (FEM-CSI) of a microwave tomography (MWT) dataset collected as part of a forearm imaging study. The data consist of field measurements taken inside a prototype MWT system that uses simple dipole antennas and a saltwater matching medium. Initial images of the 2-D cross-sectional dielectric profile of the individuals' arms are reconstructed using FEM-CSI. These initial "blind" imaging results show that the image quality is dependent on the thickness of the arm's peripheral adipose tissue layer: Thicker layers of adipose tissue lead to poorer overall image quality. The poor image quality for arms with high levels of adipose tissue is not improved by changing the matching fluid's complex dielectric constant. Introducing prior information into the FEM-CSI algorithm in the form of an inhomogeneous background consisting of an adipose layer surrounding a muscle region provides substantial improvement of the image quality: The internal anatomical features of the arm are resolved for each of the five datasets. Two methods are employed to estimate the arm periphery and adipose layer thickness from the blind imaging results: manual estimation and a novel image segmentation algorithm based on global optimization using simulated annealing.**

***Index Terms*—Contrast source inversion, inverse scattering, microwave imaging, prior information, simulated annealing.**

I. Introduction

MICROWAVE tomography (MWT) is a modality that has shown potential in various biomedical imaging applications such as breast cancer detection and monitoring [1], as well as in extremity imaging [2]. Several challenges confront the quantitative inverse scattering algorithms associated with the fully nonlinear biomedical imaging problem. One of the biggest challenges is that most biomedical objects of interest (OIs) are highly inhomogeneous with respect to the complex relative permittivity profile that is to be reconstructed. The range of permittivity values corresponding to human tissues is large, and sometimes two tissues of interest differ by only a few percent [3]. Adjacent tissues of widely differing permittivity may also shadow each other with respect to the interrogating microwave energy. This is the case, for example, when an adipose layer surrounds muscle tissue, each having a complex relative permittivity of $\epsilon_{\mathrm{r}} = 10 - j1$ and $\epsilon_{\mathrm{r}} = 50 - j20$, respectively, at 1 GHz. Add to the possible shadowing effects the large amount of multiple scattering inherent in such highly inhomogeneous regions, and it becomes clear why the nonlinear inverse scattering problem is so difficult to solve.

Here, we show that the inverse problem for a biomedical target exhibiting a large amount of inhomogeneity, the human forearm, is more effectively solved by the incorporation of prior information about some of the tissues' expected electrical properties as well as a minimal amount of information about the arms anatomical features. The experimental scattering data used in this letter was obtained as part of a pilot study that used MWT to image the forearms of five volunteers. Although the use of prior information to enhance the quality of MWT reconstructions has been investigated in the past, e.g., [4] and [5], here we make novel use of the finite-element contrast source inversion's (FEM-CSI's) ability to incorporate an inhomogeneous background medium in its forward scattering operator [6]. This procedure still allows the complex permittivity of the tissue, $\epsilon_{\mathrm{r}}(\mathbf{r})$, to be updated throughout the whole imaging domain, except that now the update is performed via a contrast variable $\chi(\mathbf{r}) \triangleq (\epsilon_{\mathrm{r}}(\mathbf{r}) - \epsilon_{\mathrm{b}}(\mathbf{r}))/\epsilon_{\mathrm{b}}(\mathbf{r})$, where the background complex permittivity $\epsilon_{\mathrm{b}}(\mathbf{r})$ is also a function of position. The closer the background $\epsilon_{\mathrm{b}}(\mathbf{r})$ prior information is to the true $\epsilon_{\mathrm{r}}(\mathbf{r})$, the smaller the magnitude of χ will be, thereby facilitating the numerical convergence of the algorithm to the correct solution.

A novel automated technique is introduced to extract the required prior information from "blind" initial inversions where no prior information is utilized. Imaging results are compared against those obtained when the prior information is estimated manually from the same blind initial inversions. In both cases, the prior information consists of an adipose layer surrounding a homogeneous muscle region.

II. Problem Configuration

A prototype MWT system was used for a pilot study where the forearms of five adult volunteers were imaged, using several frequencies and various background mediums exhibiting different amounts of loss. The imaging system consists of a circular cylinder metallic chamber of radius 22.4 cm filled to a height of 44.4 cm with a saltwater background medium. The system utilizes 24 dipole antennas with a quarter-wavelength balun as transmitters and receivers. The antennas are polarized along the axis of the cylinder, the z-coordinate, and equally distributed on a circle of radius 9.4 cm from the center of the metallic chamber. They are positioned at the midpoint height

Manuscript received October 15, 2012; revised November 19, 2012; accepted December 30, 2012. Date of publication January 03, 2013; date of current version January 31, 2013. This work was supported by the Natural Sciences and Engineering Research Council of Canada.

The authors are with the Department of Electrical and Computer Engineering, University of Manitoba, Winnipeg, MB R3T 5V6, Canada (e-mail: Joe_LoVetri@umanitoba.ca).

Color versions of one or more of the figures in this letter are available online at http://ieeexplore.ieee.org.

Digital Object Identifier 10.1109/LAWP.2012.2237537

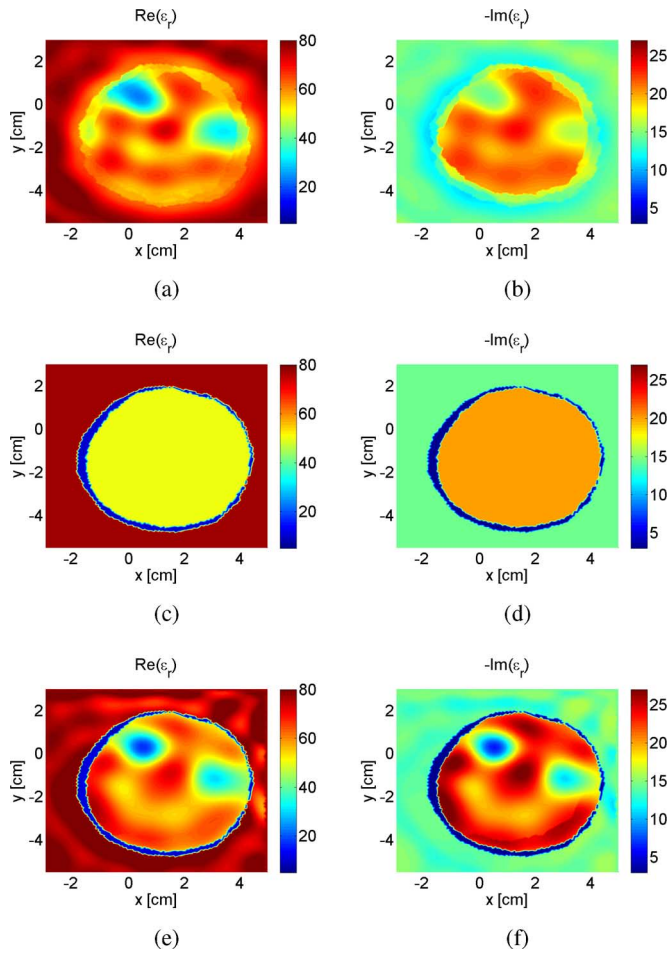

Fig. 1. Volunteer 1: (a), (b) MWT reconstruction of forearm with no prior information; (c), (d) manually estimated prior information; (e), (f) reconstruction when prior information is used as inhomogeneous background.

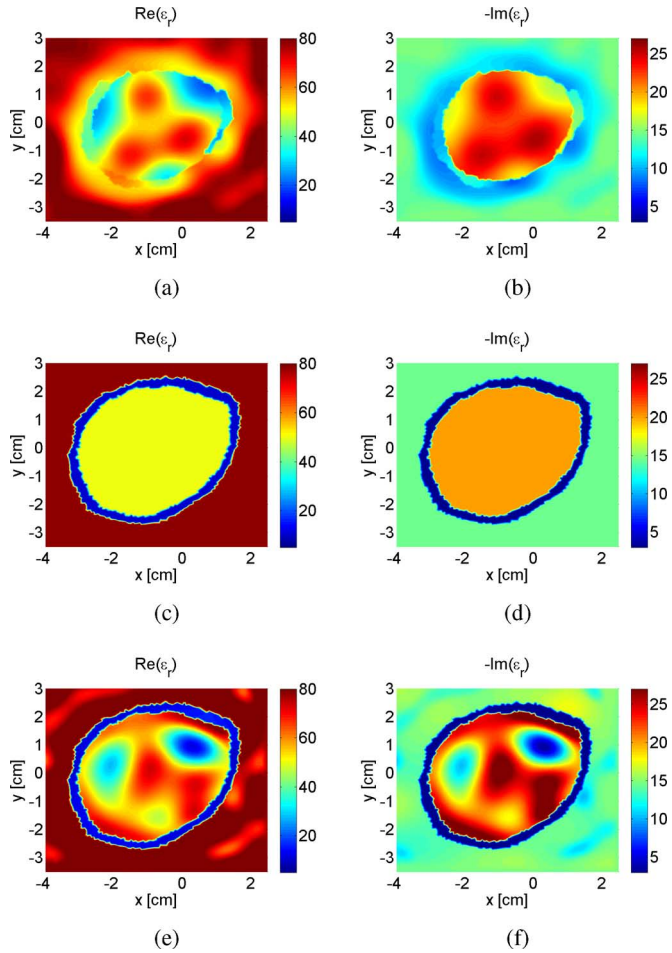

Fig. 2. Volunteer 5: (a), (b) MWT reconstruction of forearm with no prior information; (c), (d) manually estimated prior information; (e), (f) reconstruction when prior information is used as inhomogeneous background.

of the enclosure (22.2 cm). As the microwave source and receiver, the antennas are connected to an Agilent vector network analyzer (VNA) via a 2×24 matrix switch. The full system description, as well as the data calibration procedure, are detailed in [7].

A. Mathematical Formulation

The system is approximated by a 2-D time-harmonic problem with longitudinal electric field polarized along the z-axis and angular frequency ω. The OI is immersed in an inhomogeneous lossy background medium within an imaging chamber assumed to have a circular perfectly electric conducting (PEC) boundary. The OI's relative complex permittivity is given as $\epsilon_{\rm r}(\mathbf{r}) = \epsilon'_{\rm r}(\mathbf{r}) - j\epsilon''_{\rm r}(\mathbf{r})$ with $\epsilon''_{\rm r} = \sigma_{\rm eff}(\mathbf{r})/(\omega\epsilon_0)$, where $\sigma_{\rm eff}$ is the effective conductivity and ϵ_0 is the permittivity of free space.

The OI is successively illuminated within the chamber by one of T transmitters, t, and the total field, $E_t^{\rm tot}(\mathbf{r})$, is measured at R receiver locations on a circular periphery surrounding the OI (also within the chamber). A *numerical* incident field $E_t^{\rm inc}(\mathbf{r})$ is defined as the field in the presence of a numerical inhomogeneous background medium in the absence of the OI. The numerical scattered field, due to the difference in electrical properties between the OI and the background medium, is defined as $E_t^{\rm sct}(\mathbf{r}) \triangleq E_t^{\rm tot}(\mathbf{r}) - E_t^{\rm inc}(\mathbf{r})$. This numerical scattered field is governed by the scalar Helmholtz equation $\nabla^2 E_t^{\rm sct}(\mathbf{r}) + k_{\rm b}^2(\mathbf{r}) E_t^{\rm sct}(\mathbf{r}) = -k_{\rm b}^2(\mathbf{r}) w_t(\mathbf{r})$, where $k_{\rm b}(\mathbf{r}) = \omega\sqrt{\mu_0\epsilon_0\epsilon_{\rm b}(\mathbf{r})}$ is the inhomogeneous background wavenumber and $w_t(\mathbf{r}) \triangleq \chi(\mathbf{r}) E_t^{\rm tot}(\mathbf{r})$ is the contrast source.

The data are inverted using the contrast source inversion algorithm formulated using the finite element method (FEM-CSI) and regularized using a balanced multiplicative regularizer [5], [6], [8]. FEM-CSI offers the ability to incorporate the inhomogeneous background medium as prior information about the OI. The variables in the prior information region are still free variables that can be changed by the algorithm. The weighted L_2-norm total variation regularizer has edge-preserving capabilities, as well as the ability to correct the imbalance that may exist between the real and imaginary components of the OI's relative permittivity. In addition, FEM-CSI provides the ability to perform the inversion on an unstructured grid of triangular elements with varying mesh density without compromising the reconstruction quality [9]. Thus, for all the inversion examples presented herein, the discretization density of the chamber's interior is greater within the imaging domain.

III. Forearm Imaging Results

The results included herein are for two of the volunteers whose forearms exhibited quite different adipose layer

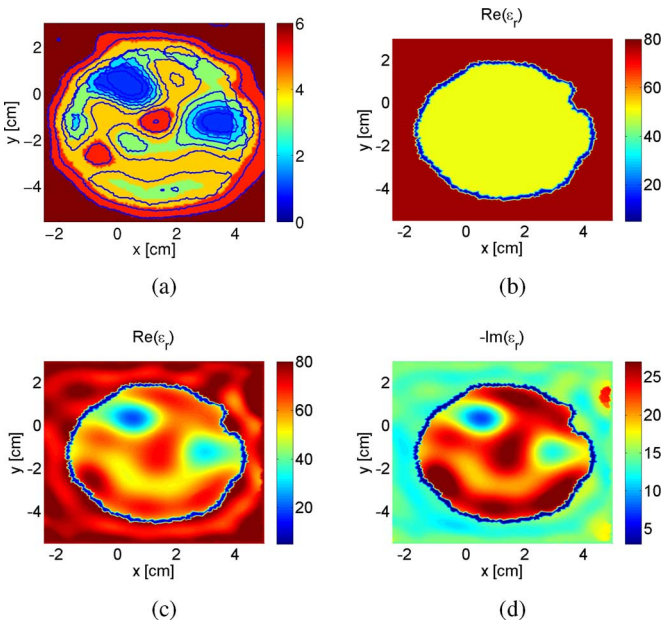

Fig. 3. Volunteer 1: (a) SA result using the blind inversion; (b) real component of estimated prior information; (c), (d) reconstruction when prior information is used as inhomogeneous background.

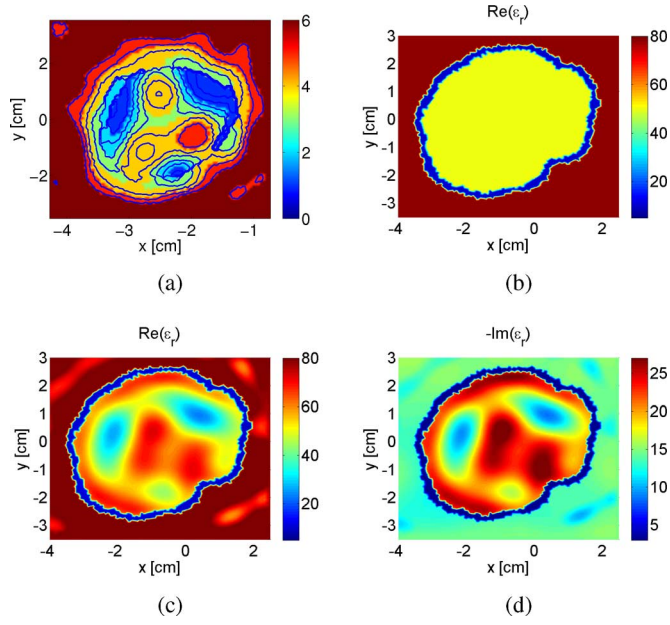

Fig. 4. Volunteer 5: (a) SA result using the blind inversion; (b) real component of estimated prior information; (c), (d) reconstruction when prior information is used as inhomogeneous background.

thicknesses (as confirmed by subsequent MRI imaging). At a measurement frequency of 1 GHz, where the permittivity of the saltwater was measured to be $\epsilon_{\rm b} \approx 77 - j15$, the real and imaginary components of the blind inversion results are shown in Fig. 1(a) and (b) for Volunteer 1 and Fig. 2(a) and (b) for Volunteer 5. While the anatomy of the first volunteer's forearm is well estimated by the inversion algorithm, the bones for the fifth volunteer are indistinguishable from the adipose layer. For both volunteers, the adipose layer thickness is not reconstructed successfully. Furthermore, the adipose layer and bones electrical permittivity values are more than the published equivalents [10].

A. Prior Information Estimation and Inversion

While incorporating prior information into the inversion algorithm is relatively straightforward, the challenge becomes developing a methodology of accurately estimating the nonuniform adipose layer. Although non-MWT-based techniques are certainly possible, in this letter two methods are used to estimate each volunteer's forearm adipose layer based solely on the blind inversion images. The first method is an *ad hoc* manual technique, whereas the second is an automated technique based on simulated annealing (SA) algorithm described below [11]. Both techniques identify three different regions within the blind inversion image: the outer background, a single adipose layer, and an inner muscle region. The numerical inhomogeneous background medium is then constructed for each volunteer's forearm assigning mesh nodes within the identified adipose layer a value of $\epsilon_{\rm r} = 10 - j1$ (taken from [10]), nodes outside the adipose layer the saltwater measured value, and nodes enclosed by the adipose layer an estimated value for muscle of $\epsilon_{\rm r} = 50 - j20$. The inversion algorithm is then rerun using the estimated prior information as a inhomogeneous background.

B. Simulated Annealing

Simulated annealing is a global optimization technique that minimizes a user-defined "energy function" $E(\mathbf{p})$, where $\mathbf{p}$ is a vector of parameters for the problem. We segment the forearm images into $M = 6$ distinct dielectric regions, each of which is assigned an integer value $m = \{1, 2, \ldots, M\}$. The algorithm begins by initializing the N pixels of a segmented image, S_n, with a random value from the parameter set $S_n \in \{1, 2, \ldots, M\}, n \in \{1, 2, \ldots N\}$. The "energy function" is defined as the statistical correlation coefficient between the vectorized image D_n and the segmented S_n [12]

$$E = \frac{s_{DS}}{\sigma_D \sigma_S} \tag{1}$$

where σ_D and σ_S are the standard deviations of D and S, and s_{DS} is the covariance between D and S.

At each iteration k, the algorithm randomly perturbs one S_n parameter to a different value S'_n, and a new energy, E', is calculated. Convergence is accelerated by choosing the value of the randomly perturbed pixel using a distribution that is biased to reflect the values of the pixel's nearest neighbors. The probability of accepting E' is $P(E') = 1$ if $E' \leq E$, and $\exp(-(E' - E/T_k))$ if $E' > E$. We initialize the cooling schedule T_k at infinity. After every 100 iterations, T_k is defined as the standard deviation of the previous 99 energies. For all other iterations, $T_k = \alpha T_{k-1}$, where $\alpha = 0.999$ is the cooling speed parameter [13]. The algorithm converges when the cooling schedule converges to some value; perturbing a single pixel no longer changes the energy appreciably.

The converged SA segmented images for volunteers 1 and 5 are shown in Figs. 3(a) and 4(a) (the contours of the original image are superimposed). The colorbars of Figs. 3(a) and 4(a) indicate the SA segmentation levels. To obtain the prior information, regions corresponding the background are set to zero. This includes the highest integer state ($m = 6$, the true

background) and the next highest state ($m = 5$), which we have found corresponds to an imaging artifact that represents a transitional area between the arm and the background. Once these levels are removed, the remaining levels are set to one, and we are left with a binary image that represents the approximate shape and location of the arm. On this binary image, we run the edge detection function *edge* from the MATLAB Image Processing Toolbox, using the Sobel approximation to the derivative. This function returns a binary image of the edges at which the gradient of the original image is a maximum. Only the longest edge is accepted as it is possible that there are holes in the binary image after removing the highest two energy values. This edge is dilated toward the center of the arm using a "two pixel" dilation to avoid an overly thin or an overestimation of the thickness of the layer. The known dielectric value for the adipose tissue is then assigned to this region. The interior muscle and exterior background values are then assigned to the two remaining regions.

C. Refinement Using CSI

After determining the initial location of the adipose layer, some refinement is required. Due to the nature of the CSI algorithm, the blind inversion image appears extended, and as a result the size of the our edge can be overestimated by the SA algorithm. If the size of the forearm is incorrect, this effect presents itself in the image as a large deviation from the known background value, which manifests itself as a saturation of the maximum allowed background value. In order to determine a more accurate size, we adjust the size of the arm, adding a row and column of background valued pixels to all sides of the image and then interpolating back onto our original sized grid; as a result, the percentage by which we reduce the arm will depend on the resolution of the original image. The CSI algorithm is run after each reduction of the forearm's size, and the percentage of pixels in the image that are saturation to the background (i.e., highest) level is calculated. The forearm size reduction is terminated when no appreciable change in this percentage occurs. The real component of the final prior information estimates are shown for both volunteers in Figs. 3(b) and 4(b). This can be compared to the manual estimation of the prior information given in Figs. 1(c) and 2(c).

IV. Discussion and Conclusion

For both volunteers, the use of the adipose layer as inhomogeneous background resulted in a substantially improved reconstruction of the forearms where the two bones can be clearly identified. Figs. 1 and 2, (c) and (d), show the manually identified prior information with corresponding inversion results in (e) and (f). The SA derived prior information and corresponding results are shown in Figs. 3 and 4. Although the two techniques provide somewhat different prior information they both lead to improved images. The algorithm qualitatively preserved the adipose layer used as prior information. The mean value of the bone's complex relative permittivity was overestimated for both volunteers in comparison to the values published in [10], nevertheless it was better estimated in comparison to the blind inversion reconstruction. The improvements were possible with minimal increase in the computational resources.

With respect to the muscle tissue, the reconstructed dielectric values are close to the *ex vivo* measurements provided in the literature [10]. As for the variations within the muscle regions, we speculate that they are due to the presence of other tissues (e.g., nerves, blood vessels, tendons, connective tissues) in the forearm.

The initial improvements in image quality demonstrated herein lead us to conclude that using a global optimization technique, such as SA, as a companion to a local optimization algorithm such as FEM-CSI is a promising way of enhancing MWT. Although the use of the SA-derived prior information as an inhomogeneous background is a straightforward and powerful enhancement, other techniques of using this information are possible and are the subject of future research. It should also be noted that the preliminary SA-based algorithm described herein does not attempt to infer the actual thickness of the adipose layer, but does a good job of determining the arm's periphery. Further improvements to the SA-based algorithm, involving the dilation step, could potentially lead to a better estimate of the thickness.

The technique described herein is applicable to other biomedical MWT applications where some anatomical feature of the OI is known—for example, the skull or skin layer.

References

[1] P. M. Meaney, M. W. Fanning, T. Raynolds, C. J. Fox, Q. Fang, C. A. Kogel, S. P. Poplack, and K. D. Paulsen, "Initial clinical experience with microwave breast imaging in women with normal mammography," *Acad. Radiol.*, vol. 14, no. 2, pp. 207–218, Feb. 2007.

[2] S. Semenov, J. Kellam, Y. Sizov, A. Nazarov, T. Williams, B. Nair, A. Pavlovsky, V. Posukh, and M. Quinn, "Microwave tomography of extremities: 1. Dedicated 2D system and physiological signatures," *Phys. Med. Biol.*, vol. 56, no. 7, pp. 2005–2017, Apr. 2011.

[3] M. Lazebnik, D. Popovic, L. McCartney, C. Watkins, M. Lindstrom, J. Harter, S. Sewall, T. Ogilvie, A. Magliocco, T. Breslin, W. Temple, D. Mew, J. Bookse, M. Okoniewski, and S. C. Hagness, "A large-scale study of the ultrawideband microwave dielectric properties of normal, benign and malignant breast tissues obtained from cancer surgeries," *Phys. Med. Biol.*, vol. 52, no. 20, pp. 6093–6115, Oct. 2007.

[4] A. Fhager and M. Persson, "Using a priori data to improve the reconstruction of small objects in microwave tomography," *IEEE Trans. Microw. Theory Tech.*, vol. 55, no. 11, pp. 2454–2462, Nov. 2007.

[5] A. Zakaria, C. Gilmore, and J. LoVetri, "Finite-element contrast source inversion method for microwave imaging," *Inverse Probl.*, vol. 26, no. 11, Nov. 2010.

[6] A. Zakaria and J. LoVetri, "Application of multiplicative regularization to the finite-element contrast source inversion method," *IEEE Trans. Antennas Propag.*, vol. 59, no. 9, pp. 3495–3498, Sep. 2011.

[7] C. Gilmore, A. Zakaria, S. Pistorius, and J. LoVetri, "A study of matching fluids loss in a biomedical microwave tomography system," *AAPM Med. Phys.*, vol. 40, no. 2, Feb. 2013, to be published.

[8] A. Zakaria, C. Gilmore, S. Pistorius, and J. LoVetri, "Balanced multiplicative regularization for the contrast source inversion method," in *Proc. 28th Int. Review Prog. Appl. Comput. Electromagn. Conf.*, Columbus, OH, 2012.

[9] A. Zakaria and J. LoVetri, "A study of adaptive meshing in FEM-CSI for microwave tomography," in *Proc. 14th Int. Symp. Antenna Technol. Appl. Electromagn. Amer. Electromagn. Conf.*, Ottawa, Canada, 2010, pp. 1–4.

[10] C. Gabriel, S. Gabriel, and E. Corthout, "The dielectric properties of biological tissues: III. Parametric models for the dielectric spectrum of tissues," *Phys. Med. Biol.*, vol. 41, no. 11, pp. 2271–2294, Nov. 2000.

[11] D. Bertsimas and J. Tsitsiklis, "Simulated annealing," *Stat. Sci.*, vol. 8, no. 1, pp. 10–15, Feb. 1993.

[12] J. Fiege, B. McCurdy, P. Potrebko, H. Champion, and A. Cull, "A novel evolutionary optimization approach to multiobjective IMRT planning," *Med. Phys.*, vol. 38, no. 1, pp. 5217–5229, Sep. 2011.

[13] Y. Nourani and B. Andresen, "A comparison of simulated annealing cooling strategies," *J. Phys. A, Math. Gen.*, vol. 31, no. 41, pp. 8373–8385, Aug. 1998.